IAC-10.A3.5.8

LANDING AND MOBILITY CONCEPT FOR THE SMALL ASTEROID LANDER MASCOT ON ASTEROID 1999 JU3

C. Dietze
Institute of Space Systems, German Aerospace Center (DLR), Bremen, Germany,
current Email: claudia.dietze@esa.int

F. Herrmann, S. Kuß
Institute of Robotics and Mechatronics, German Aerospace Center (DLR), Oberpfaffenhofen, Germany

C. Lange, M. Scharringhausen, L. Witte, T. van Zoest
Institute of Space Systems, German Aerospace Center (DLR), Bremen, Germany

H. Yano
Department of Planetary Science, Institute of Space and Astronautical Science, Japan Aerospace Exploration
Agency, Sagamihara, Japan

To enhance the currently studied asteroid sample return mission HAYABUSA-2 by in-situ science the Institute of Space Systems of the German Aerospace Center (DLR) is in lead of a proposal for a lander called MASCOT (Mobile Asteroid Surface Scout). Its mass of 10 kg lies in between those of the HAYABUSA small lander MINERVA (1 kg) and the legged ROSETTA comet lander PHILAE (100 kg). In the successfully completed feasibility study the design of the MASCOT converged to a landing package with 10 kg total mass, 3 kg of payload and the capability of hopping. As a result of its reduced size and the highly demanding constraints regarding e.g. mobility, the design as well as the landing and mobility cannot be adapted from MINERVA and PHILAE.

This paper is intended to give an overview over the demanding landing and mobility concept for MASCOT. The current MASCOT baseline design is presented, which has to deal with tight budgetary limitations leading to a consolidated and widely integrated design, while still offering excellent performance in terms of mobility and resulting science. The focus lies on the mission analysis tasks and the mobility concept, which is studied in detail during the ongoing preliminary design phase. The general mission constraints including the parameters of the target asteroid (162173) 1999 JU3 are presented, while emphasis is put on the modelling of the asteroid's inhomogeneous gravity field. Therefore different gravitational models are implemented and their effect on the descent trajectory is compared. Of equal importance is the design support by investigating the two major mobility aspects, i.e. the self-uprighting mechanism and hopping over the asteroid's surface. These two issues are studied by applying both multi-body system and contact dynamics approaches. Moreover, this analysis will support the design of the actuator system for uprighting and hopping. After a presentation of the surface modelling and simulation approach an overview over first results and a short outlook on future mobility analysis and test activities for MASCOT is given.

I. INTRODUCTION

Small, primitive bodies like asteroids and comets remained nearly unaltered since the planetary formation process and therefore can provide unique information about our solar system and the origin of life. Returned surface samples are intended to give a detailed insight, thus several asteroid sample return missions to near-Earth objects are studied worldwide. In the frame of the European Cosmic Vision 2015-2025 Program, ESA studied the MARCO POLO mission, which was postponed during the down selection of M-class missions at the beginning of this year. In parallel, a mission study of a successor of the Japanese HAYABUSA spacecraft, which returned to Earth in June 2010, is performed by JAXA. The Institute of Space Systems of the German Aerospace Center (DLR) in cooperation with other institutes proposed early in their respective study phases a small landing package called MASCOT (Mobile Asteroid Surface Scout) to complete these sample return mission by in-situ science.

The MASCOT concept is suitable for both missions, considering design as well as mission constraints, although the currently envisaged opportunity is HAYABUSA-2.

Landing and mobility on a small body implies several challenges and is very different to planetary missions [1]. The particularities derive on one hand from the small dimensions resulting in very low gravity, which leads to a high escape risk from the body, and (depending on the surface properties) resulting in a dynamically touch-down in terms of re-bouncing. On the other hand, making it even more difficult to design a small-body lander, the properties of these bodies are widely unknown and the few visited bodies show a wide range. The shape and rotational state can be irregular resulting in a complex gravity field, whereas the surface properties, which mainly affect mobility, will even differ across the surface of one asteroid. The target body's properties are not known precisely until arrival, thus meaning high uncertainty during the design of the lander.

In the following the MASCOT baseline design, is presented with a more detailed discussion of the robust landing and mobility concept thereafter.

II. MASCOT BASELINE DESIGN

The lander MASCOT was investigated in the framework of the European MARCO POLO mission, for which it was recommended for study as the result of the response to the Declaration of Interest (DOI) call in 2008. During two dedicated studies in the Concurrent Engineering Facility (CEF) at DLR Bremen the lander concept converged to a small landing package, i.e. an unlegged lander, of 10 kg that would perform a passive descent from main spacecraft. This system design was later identified to be also suitable for the Japanese HAYABUSA follow-up mission, for which MASCOT was studied in parallel following an invitation from JAXA. In January 2010 a detailed, third CE-study succeeded, while the phase-A study will be completed by the end of July 2010.

Compared to previously designed small-body landers, i.e. the Japanese MINERVA lander on HAYABUSA s/c and the European PHILAE lander for ROSETTA mission, the MASCOT landing package provides a good compromise of a low mass system with still extensive P/L capability. While MINERVA is a very small (100 mm height, 120 mm diameter) and light-weighted (1 kg), cylindrical landing package with the ability to hop by rotation of an internal torquer, the PHILAE lander, a legged landing system developed under lead of DLR marks the other side of the interval with a mass of 96 kg. The MINERVA lander was designed to investigate the surface of the target asteroid 25143 ITOKAWA with CCD cameras, Sun sensors and thermometers, but unfortunately the lander, which was relying on the main s/c for the targeting of the landing site and the deployment, got lost during this phase and/or the subsequent passive descent to the asteroid surface. [2]

Fig. I: HAYABUSA-2 s/c and MINERVA hopping robot (artist view) [3]

PHILAE will perform an active descent with a final anchoring, but has no mobility on the surface of comet 67P/Churyumov-Gerasimenko. With the 26 kg of scientific payload, the lander will bring new knowledge after its delivery at end of 2014. [1]
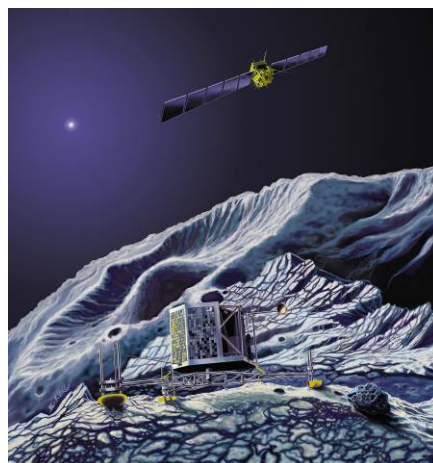

Fig. II: ROSETTA s/c and PHILAE lander on comet surface (artist view)

II.I. Science Case

A dedicated, mobile lander provides a local study of the surface and in-situ measurements at different sites, which accounts for its probable heterogeneity and can't be performed by other means. This allows bringing the global, remote sensing investigations of the main s/c and the microscopic analysis of the returned samples in a comprehensive science context. A three-fold role of MASCOT can be derived [4]:

1) **Context Science**, i.e. filling the gap between the global science from main s/c and the sample return investigations.
2) **Stand alone science**, which describes the unique in-situ measurements only possible by a landing system, e.g. geophysics, analytical characterisation of elemental, isotopic and molecular composition of surface material in its natural state as well as astrobiological investigations.
3) **Reconnaissance and scouting** stands for the evaluation of sites prior to the main s/c landing in order to identify interesting sampling sites.

A variety of instruments were proposed by the science community to fulfil these goals, whereupon a subset of three instruments was chosen by reason of the strict mass limitation based on their scientific objectives and the compliance with the overall mission science objectives and requirements. This 3 kg set comprises [5]:

- ILMA (Ion Trap Mass Spectrometer) or XRD/XRF or Bi-static radar of 2 kg
- VIS and Infrared Microscope of 0.7 kg
- Wide Angle Camera of 0.3 kg

II.II. Requirements and Systems Overview

Based on the challenging requirements that are imposed to a landing package due to the asteroid environment (e.g. temperature conditions, radiation and signal roundtrip time) as well as the constraints for the design given by the main s/c (mass and physical envelope), the baseline design for the MASCOT lander, as established and commissioned

during the CE-studies in 2009 and early 2010, is specified as follows:

- **Mission:** launch 2014/15, deployment June-August 2019, release altitude 100 m, 16 hrs of on-asteroid operation
- **Main functions:** on-surface uprighting and mobility (incl. attitude determination) and mainly autonomous science measurements and operation without ground interference
- **Mass:** 13.5 kg including all margins and interface parts remaining on the main s/c
- **Physical envelope:** 0.3 x 0.3 x 0.2 m^3
- **Configuration:** prismatic body with highly integrated accommodation, fixed instrument placement, integrated electronics compartment/ common E-box, no attitude control, no attitude stabilization during descent
- **Structure:** aluminium-based support structure and casing with sandwich base and top plate
- **Mechanisms:** separation mechanism (relative to main s/c) and a mobility mechanism for uprighting and hopping
- **Thermal:** mainly passive (i.e. using coatings and MLI) with heating only during cruise and for warm-up
- **Power:** primary battery only for 160 Whrs (solar generators are optional)
- **Communication:** redundant, omni-directional UHF-Band link between MASCOT and main s/c with the option of using synergies with other landers and the main s/c
- **DHS:** redundant on-board computer
- **Attitude determination:** on-board sensors for determining movement and on-surface attitude
- **Redundancy concept:** consider redundancy for onboard computer

A mass breakdown of the current system configuration is shown in Table I.

	Dry Mass [kg]	Eff. Margin %	Wet Mass [kg]
Structure	2.90	0.0	2.90
Thermal Control	0.41	15.4	0.47
Mechanisms	0.48	17.8	0.57
Communications	0.36	10.0	0.40
DHS	0.40	20.0	0.48
Power	1.00	12.0	1.12
Harness	0.30	20.0	0.36
Payload	3.00	0.0	3.00
Attitude Determination	0.20	20.0	0.24
Landed Mass	9.1		9.5
Interface Parts	1.5	13.0	1.7
Subtotal			11.3
Total incl. 20% System Margin			13.5

Table I: Mass breakdown table

For each subsystem, the dry mass is given based on the expert estimations. In addition to that, an effective margin is applied, which is based on the internal standard for CE-studies and uses 5%, 10% and 20% margins for fully developed items, items to

be modified and items to be developed respectively. The total mass of the lander including all margins has been estimated of being 9.5 kg. In addition to that, interface parts remaining on the main s/c have been sized, which include e.g. an electrical support system and the release mechanism. The subtotal mass of the landed system and the parts remaining on the main s/c of 11.3 kilograms is increased by a final system margin of 20%, which is a standard for a phase-A study as well. This leads to the total estimated mass of 13.5 kg.

Fig. III shows the current configuration of the lander. A more detailed description of the subsystems design is given in [5].
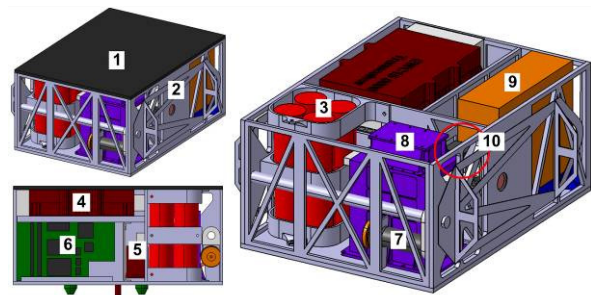

Fig. III: MASCOT configuration isometric and side view with (1) sandwich top plate, (2) main aluminium structure (3) battery pack, (4) transceiver unit and (5) Rx-filter, (6) common E-box, (7) motor and gear for the mobility mechanism, (8) MicroOmega, (9) ILMA, (10) Camera

III. MISSION ANALYSIS

Most MASCOT activities naturally depend on the HAYABUSA-2 mission timeline, which lead to a close collaboration between the Japanese HAYABUSA-2 and the MASCOT team. The follow-on mission will be finally approved this year with an envisaged launch in 2014 [6]. After the arrival in June 2018 the global characterization will start, while the s/c will fly nearby the asteroid on a virtual line from 1999 JU3 to the Sun similar to HAYABUSA. This constellation results from the stationary solar arrays and leads to the assumption that the global characterization phase will last half the asteroid orbit due to the highly declined asteroid rotation axis (ecliptic latitude of 20 deg [7]).

For safety reasons HAYABUSA-2 will perform its sampling dress rehearsal manoeuvres subsequently to a completed observation of the asteroid [8], i.e. after the global shape and gravity field have been determined. The combination of the requirement of being deployed during one of these descents and thermal restrictions on the system design. i.e. too high asteroid surface temperatures around the solstice in April 2019 [9], the lander deployment has been estimated to take place in a timeframe from June 2019 till August 2019, but latest before the Japanese impactor experiment takes place. The Fig. IV shows the overall mission timeline.
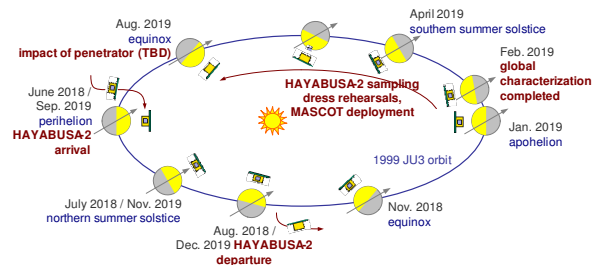
Fig. IV: HAYABUSA-2 and MASCOT overall mission timeline

III.I. Mission Description

The landing site is selected prior to the MASCOT deployment by evaluating the global asteroid map, but is restricted to the illuminated asteroid side. During a sampling dress rehearsal manoeuvre the main s/c will stepwise descent from its Home Position (HP) to an altitude of approx. 100 m and deploy the lander by initializing a Δv through the separation mechanism. The lander free-falls to the surface while HAYABUSA-2 will ascend back to its HP at 15 km distance [10]. Permanent communication between MASCOT and HAYABUSA-2 is foreseen during the 20…30 min of descent. The Fig. V shows a schematic of the MASCOT deployment.

Fig. V: Deployment phase

After touchdown around local noon the lander could bounce due to the low gravity ($g \approx 10^{-4}$ m/sec²), finally it comes to rest in an arbitrary attitude. The up-righting mechanism will ensure a correct positioning to the surface (for instruments, communication, thermal etc.). The remaining daytime will be used to perform the first science operation cycle with those instruments requiring (or allowing) illumination, while in parallel the access to HAYABUSA-2 s/c is used for communication to Earth (with 13-20 min of signal propagation delay from asteroid to Earth).

With approaching night-time the access gets lost and the data of scientific investigations performed at night has to be stored until the next access during the next asteroid day. At some point in night-time after completion of the first experiment cycle at the primary landing site, a relocation manoeuvre is performed. Following the uprighting sequence (if necessary), the second measurement cycle at the second landing site starts. The described phases will repeat until the end of MASCOT's lifetime after 15 hrs of operation.

III.II. Modelling of Gravity for Target Asteroid 1999 JU3

The characteristics of the selected target asteroid 1999 JU3, which was observed from Earth during a dedicated campaign in 2007/08, are listed in the following Table II. Two dimensions were considered for robustness (effective diameter d of 920 m and 980 m respectively) and an ellipsoid was assumed as depicted in Fig. VI.

effective diameter	920 m	980 m
ratio of semiaxes		1.3 : 1.1 : 1
dimension (semiaxes)	460 m x 390 m x 350 m	490 m x 415 m x 375 m
volume	$2.6 \cdot 10^{8}$ m³	$3.2 \cdot 10^{8}$ m³
density		1 300 kg/m³
mass	$3.4 \cdot 10^{11}$ kg	$4.2 \cdot 10^{11}$ kg
gravitational parameter μ	22.8 m³/sec²	27.7 m³/sec²
escape velocity	31.5 – 36.1 cm/sec	33.6 – 38.3 cm/sec
rotation period		7 h 37 min 38 sec
spin axis orientation		λ = 331 deg, φ = 20 deg (J2000 Ecliptic frame)

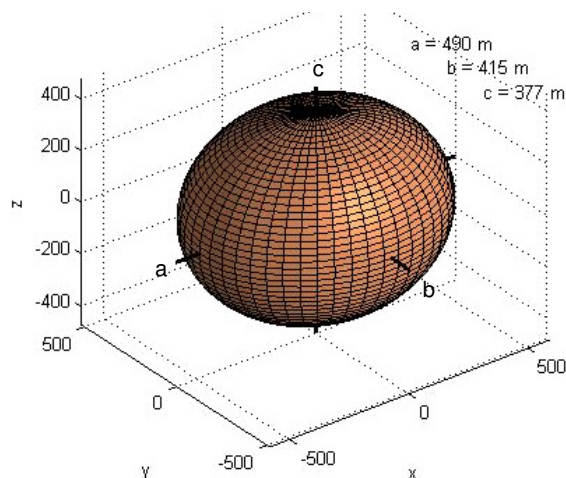Table II: 1999 JU3 asteroid characteristics [7], [11] [12]

Fig. VI: Tri-axial ellipsoidal asteroid with the body semiaxes a, b, c

In accordance with the assumed ellipsoidal body shape the resulting gravity field was computed with Carlson's elliptical integrals [13], [14]. The Fig. VII and Fig. VIII show the gravitational acceleration for an ellipsoidal asteroid with $d = 920$ m on a reference sphere with the same diameter and the decreasing gravitational acceleration with increasing altitude along the three asteroid body main axes (descent at a/b/c) respectively.
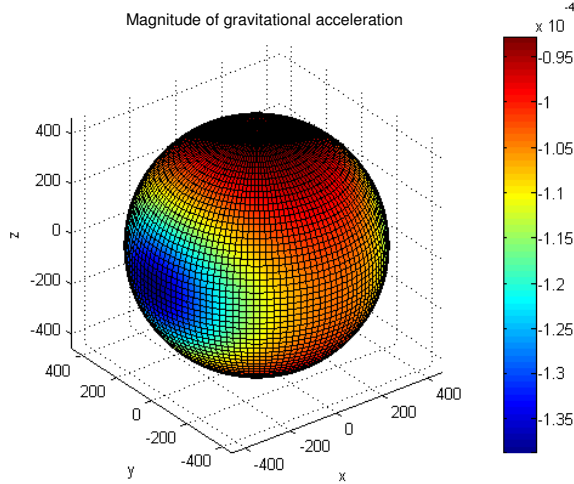

Fig. VII: Gravitational acceleration of ellipsoidal asteroid with $d = 920$ m on reference sphere with same radius
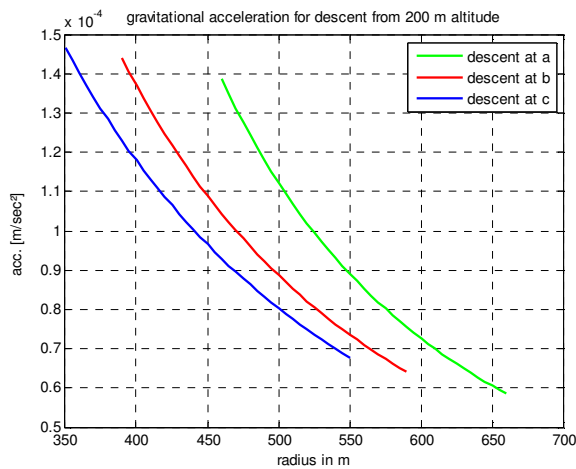

Fig. VIII: Gravitational acceleration vs. altitude for ellipsoidal asteroid with $d = 920$ m

A preliminary mission analysis used a series expansion approach with spherical harmonic coefficients to model the gravity. Its main drawback is the decreasing accuracy with increasing proximity (see following diagrams) and the divergence inside the reference sphere (that surrounds the body and holds $r_{ref} = d/2$). The following Fig. IX and Fig. X visualize the difference in the gravitational attraction between this and the before described mathematical approach.
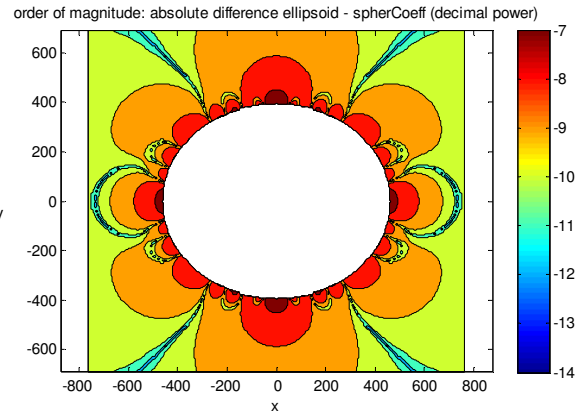

Fig. IX: Order of magnitude of absolute difference in gravitational acceleration between approach with elliptical integrals and spherical harmonics
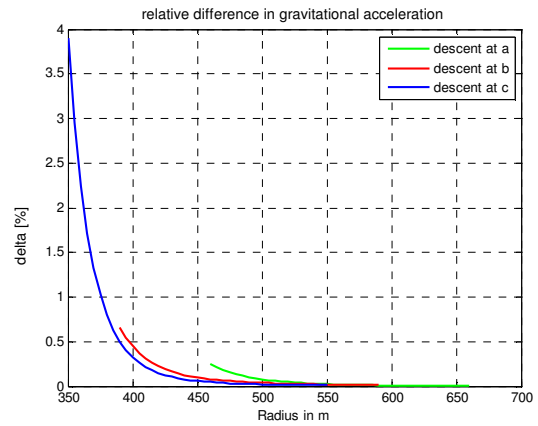

Fig. X: Relative difference in gravitational acceleration depending on altitude ($d = 920$ m)

The asteroid's gravity is the main force acting on the lander during descent (order of magnitude of 10^{-4} m/sec² compared to 10^{-8} m/sec² from solar radiation pressure and 10^{-11} m/sec² due to 3rd body perturbations), thus different gravity fields result in differing trajectories. In the low altitude range, where the landing takes place, this variation could be serious due to entering the reference sphere. But as simulations showed, for a slightly ellipsoidal body like the implemented model for 1999 JU3 there are only small deviations in the range of < 1 m (see Fig. XI) and < 0.2 cm/sec. The reason is the small penetration depth h_{enter} of the reference sphere ($h_{enter}/r_{ref} < ¼$). The larger divergence for a near polar landing ('descent at lat70deg a' and 'descent lat70deg b' denote a landing at a latitude of 70 deg in direction of the corresponding body axis) compared to the equatorial ones ('descent at a', 'descent at b') can also be seen in the diagrams below (Fig. XI and Fig. XII). Fig. XIII compares the trajectories computed in the two different gravity fields for a descent at the semi-major axis a.
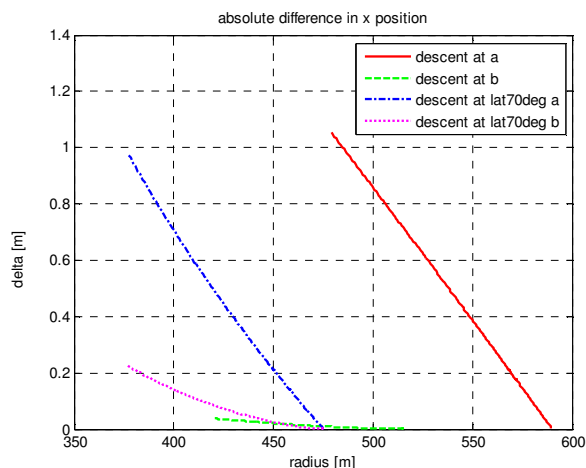
Fig. XI: Absolute difference of descent trajectories in x-direction due to different gravity models (d = 980 m, spherical harmonics up to degree and order 5)
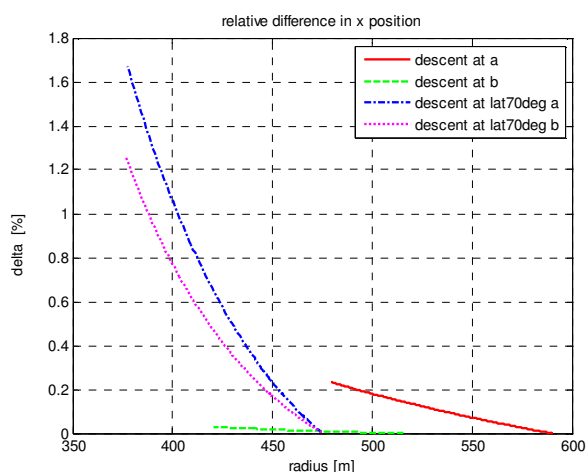

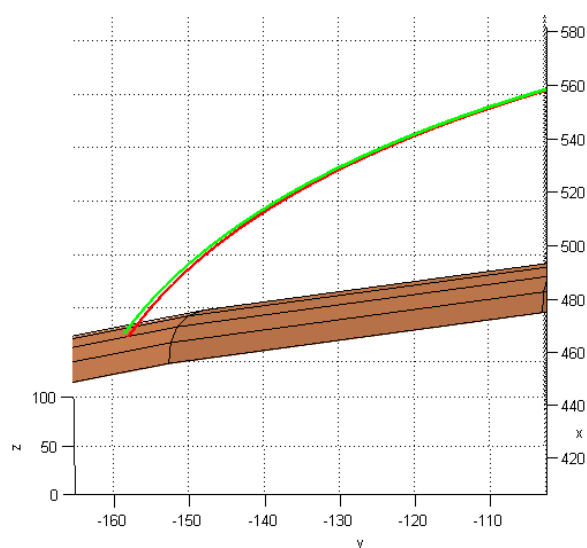Fig. XII: Relative difference of trajectories in x-direction

Fig. XIII: Descent trajectories at semi-major axis a in gravity field modelled by elliptic integrals (red) and spherical harmonics (green), d = 980 m

III.III. Separation, Descent and Landing Analysis

For safety reasons, the landing velocity was restricted to less than 50% of the escape velocity, resulting in a limitation of the separation altitude h_{sep} and velocity Δv. The maximum allowed altitude lies in the range of 98 – 144 m for the smaller and 105 – 153 m for the bigger asteroid. These values correspond to the defined maximum separation altitude of 100 m for MASCOT. The envisaged $\Delta v \approx 3$ cm/sec is feasible, yielding to nominal descent duration in the range of 25 – 30 min.

From mission analysis point of view, the HAYABUSA-2 s/c mainly affects MASCOT during the deployment phase (besides the timely mission constraints), i.e. by the possible separation altitude and attitude as well as by its position and navigation accuracies. The latter result in landing site dispersion, which has been calculated with the following accuracies:

vertical position accuracy	3 m
lateral position accuracy	10-30 m
velocity accuracy	3-4 cm/sec
attitude accuracy	0.1 deg
separation Δv	10%
separation direction	0.5 deg

Table III: Position and navigation accuracies assumed for HAYBUSA-2 s/c and MASCOT separation [8]

In March 2009 a preliminary landing analysis for impacting in a region near the middle-axis was conducted by JAXA (see [10], [15]). At that time a vertical deployment of MASCOT and a significant smaller velocity error for HAYABUSA-2 s/c of 1 cm/sec were assumed, resulting in a smaller calculated size of the landing ellipse than the current one. The present lateral deployment combined with the higher lateral velocity error of the main s/c (which equals the separation Δv itself) leads to bigger landing site dispersion as determined before. Results are presented below:

asteroid dimension	d = 920 m	d = 980 m
descent duration	18-39 min	17-36 min
landing velocity	15-19 cm/sec	15-19 cm/sec
landing ellipse total linear dimension	180 m x 240 m	170 m x 230 m
landing ellipse total angular dimension	$\Delta\varphi$ = 24 deg $\Delta\lambda$ = 31 deg	$\Delta\varphi$ = 21 deg $\Delta\lambda$ = 28 deg

Table IV: Landing site dispersion

The latitudinal dimension $\Delta\varphi$ of the landing ellipse has to be accounted for, when determining the separation window wrt. thermal environment. The

longitudinal extension $\Delta\lambda$ influences the local time of landing. A difference of 31 deg in longitude of the landing place results in a local time variation of 39 min, whereas 28 deg corresponds to a local time delay of 30 min.

The ratio of the landing ellipse dimensions d_{LE} of MASCOT compared to the asteroid dimensions for 1999 JU3 are in the range of that of HAYABUSA at asteroid 25143 ITOKAWA (d_{LE}/d = 0.2-0.3). A GNC accuracy circle of 60 m diameter was envisaged for HAYABUSA touchdown [16] on the smaller target asteroid with dimensions 535 m x 294 m x 209 m [17].

The pictures in Fig. XIV show the landing site dispersion of a Monte Carlo simulation with 5000 runs, where the accuracies listed in Table III were assumed as 3-σ values. Uncertainties regarding the asteroid were considered by investigating two body dimensions, as listed in Table II.
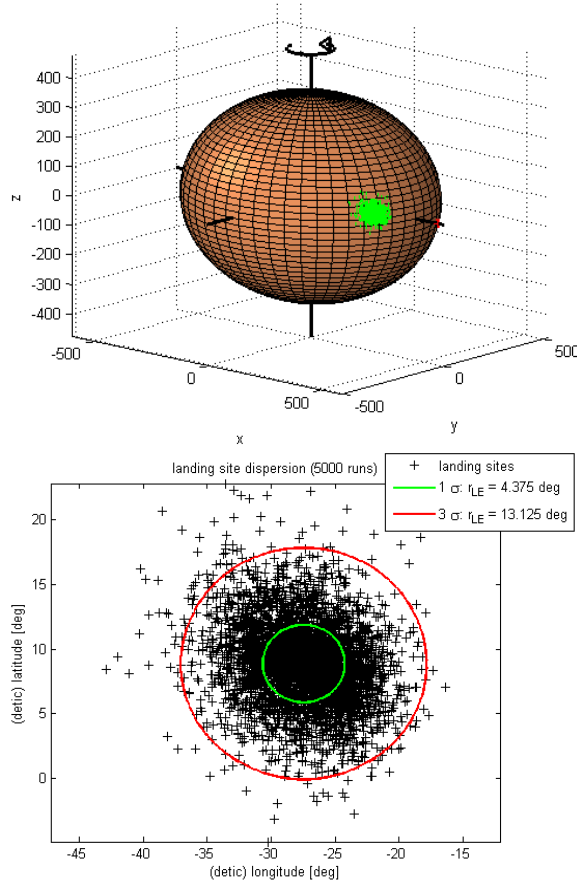

Fig. XIV: Landing site of 5000 Monte Carlo runs, h_{sep} = 100 m, descent at a, d = 920 m

A landing at the asteroid side with the biggest radius (semi-major axis a) is most challenging due to the low escape velocity v_{escape} there.

$$v_{escape} = \sqrt{\frac{2 \cdot \mu}{r}} \qquad [1]$$

If applicable, a landing site with a preferably small radius r should be selected. Nevertheless, the MASCOT landing concept is highly robust and allows

due to its simplicity, to have additional mobility on the surface as is described in the following (and was analysed by DLR in Oberpfaffenhofen).

IV. MOBILITY ANALYSIS

The mobility subsystem has to provide two operation modes: The first is an uprighting mode to bring MASCOT in nominal attitude for the payload instruments, the second a hopping mode for relocation to provide the possibility to perform measurements on different sites on the asteroid. For an effective application on the asteroid's surface the special conditions there have to be taken into account. Therefore the system has to be applicable under microgravity as well as on the widely unknown asteroid surface, which can consist of and change between hard, rocky terrain and soft soil.

These uncertainties make it essential to support the design development by detailed mobility dynamics investigations, based on efficient multibody simulations, which give an overall system view for different mission scenarios and environment conditions.

IV.I. Requirements

The task of the uprighting mode is to provide the capability to upright from any random on-surface attitude, while the hopping or re-location mode intends the possibility to change the position of MASCOT on the asteroid. The uprighting mode is the primary one and relevant for the mission success by bringing the scientific equipment and antennas to nominal attitude. The mobility system has to manage a highly robust motion with respect to uncertain and different soil properties including gravel, rocks and soft soil. This can be achieved by finding a system, which is as independent from surface interaction as possible. The hopping velocity must not exceed 50% of the escape velocity on the asteroid's surface. Therefore adjustability to different scenarios has to be implemented to ensure the limited velocity. The mechanical construction should on the one hand be of low complexity for overall mass and power-budget reasons. On the other hand it must be resistant against environmental conditions on the asteroid such as dust and sand as well as vibration and radiation during the start and delivery phase.

IV.II. Concepts

It was decided to change the baseline concept from the arm concept, which was favoured in the past [18], to a concept which uses an excentric mass to move MASCOT. This step was made according to an additional trade off study using simulation results. The two concepts and reasons for changing are presented in the following.

Arm concept

This concept uses arms on both sides of MASCOT. The arms are driven by a motor-gearbox unit to upright or to lift off the MASCOT structure by

pushing it off the ground. The motor is connected via a high ratio gearbox to an axle, which rigidly connects both arms.
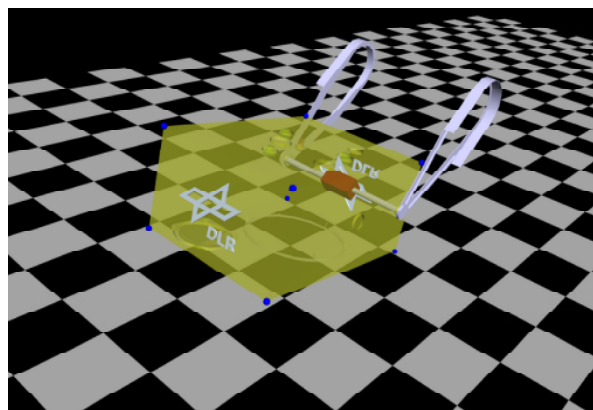

Fig. XV: Arm concept: MBS configuration

The upright mode is realized by a very slow rotation of the arms, which come into contact with the ground to turn the MASCOT structure. To achieve a re-location, the arms are brought into faster rotation, which results in a push-off of MASCOT from the ground. Fig. XV shows the virtual configuration of the arm concept in the MBS (Multi Body System) simulation.

One advantage of this concept is the possibility of a moving adaption by different arm moving sequences. Another is the advanced design progress (TRL) resulting from previous investigation and design work by DLR in Bremen [18]. Generally, this concept allows a simple motor and controller design.

However, there are also disadvantages identified. The movement is dependent on the contact of the small area where the two arms touch the surface. As the ground condition is hardly known, the resulting movement can not be determined from the arm sequence. It is imaginable that the arms have different contact conditions or even one or both arms get stuck into rocks or a gap. Beside the critical contact problem on the asteroid it is of certain effort to safely fix the arms during the transport flight and get them working on the asteroid.

Excenter tappet concept

The excenter tappet concept uses one or more masses, which are excentrically mounted on a tappet. A possible design is shown in the MBS configuration in Fig. XVI and Fig. XXVII (section IV.V.). The masses on each side are accelerated and decelerated by the actuator in a controlled way. A defined stop of the masses generates the momentum, which makes MASCOT rotating or pushing itself off the ground.
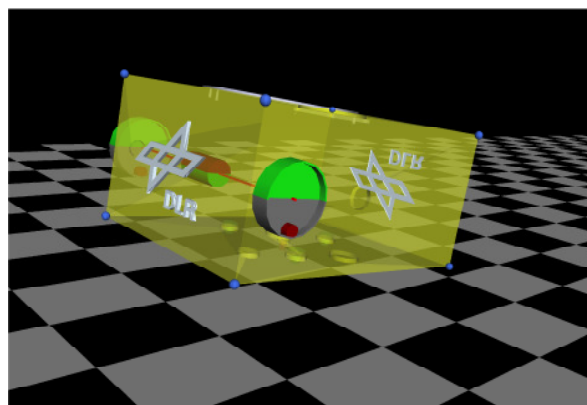

Fig. XVI: Excenter tappet concept: MBS configuration

This concept has, as the arm concept does, the advantage of providing adaptive moving with only one actuator by implementing different actuator sequences. As the concept uses a momentum for movement, instead of a repulsion using a small contact area, it has the advantage of being more independent from soil characteristics. Furthermore, the danger of getting stuck is widely avoided by the now possible compact, closed shape design of the MASCOT structure.

IV.III. Soil parameters

For purposes of breadboard testing, verification and validation of multi-body simulations, reference soils have to be defined. These soils shall reflect the multitude of soil surface conditions being possible to be encountered on the surface of 1999 JU3. In total four reference soils (MRS: MASCOT Reference Soils) have been defined:

- MRS-A : fine sand, a mixture of Olivine ($(Mg, Fe)_2SiO_4$) and regular dry quartz sand (SiO_2)
- MRS-B : intermediate, dry quartz sand
- MRS-C : coarse (i.e. fine flint)
- MRS-D : pebbly (i.e. coarse flint)

The grain size distributions for MRS-A and MRS-B are given in Fig. XVII, Fig. XVIII and Table V. The MRS-C and MRS-D soil exhibit a uniform grain size distribution of 0.7 – 1.5 mm and 8 – 12 mm, respectively.
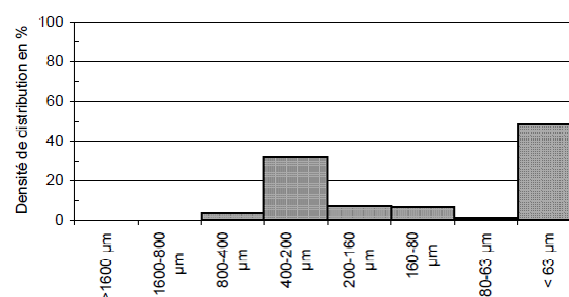

Fig. XVII: Graphical visualization of grain size distribution (weight fractions) for fine sand, proposed to be reference soil MRS-A.

Gammes des tamis	Densités de distribution (%)
>1600 µm	0,00
1600-800 µm	0,02
800-400 µm	3,90
400-200 µm	32,05
200-160 µm	7,55
160-80 µm	7,00
80-63 µm	1,13
< 63 µm	48,35

Table V: Numerical values of grain size distribution (weight fractions) for fine sand, proposed to be reference soil MRS-A.
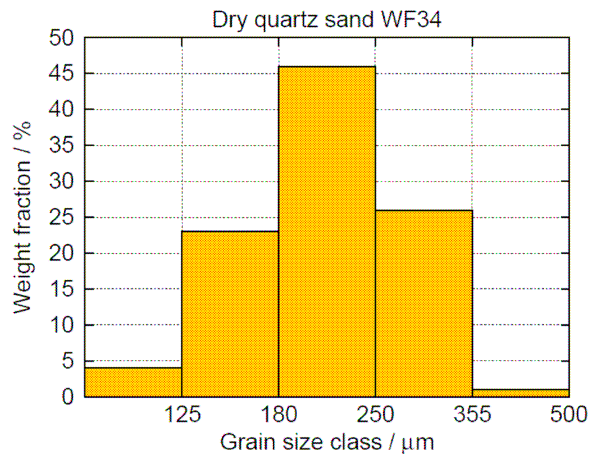

Fig. XVIII: Grain size distribution (weight fractions) for dry quartz sand, proposed to be reference soil MRS-B.

These soils are characterized by a set of parameters being common in soil mechanics. These parameters reflect both the shear and the loading strength of the respective soil [19]. That is, for loading stress, the following relationship between sinkage z and pressure p is appropriate:

$$p(z) = k^* \times z^n \qquad [2]$$

Note that both k^* and n depend on the area and shape of the loading plate. The parameters listed in Table VI: are in reference to a circular loading plate of 10 – 20 cm diameter.

For shearing stress, the maximal shear stress that can be applied to the soil before soil layers start to move against each other is given by:

$$\tau = c + \sigma \cdot \tan(\phi) \qquad [3]$$

Here, σ denotes the normal load, c the cohesion and ϕ the angle of internal friction.

It should be noted that the values given in Table VI: are to be considered preliminary, as the actual properties of the reference soils will be measured as soon as the soils are physically available.

	MRS-A	MRS-B	MRS-C	MRS-D
Soil class	fine	intermediate	coarse	pebbly
Grain size dist. / mm	Fig. XVII, Table V	Fig. XVIII	0.7 – 1.5	8 – 12
Bulk density / kg/m^3	1300 – 2300	1400	1800	1800
Internal friction angle / deg	30 - 32	31 - 33	30 - 39	20 - 30
Cohesion / kPa	1.0	0.0	0.0	0.0
Deformation coefficient n (no unit)	1.1 – 1.8	0.8 – 1.5	1	1
Scaling coefficient k^* / kN/m^{n+2}	10^3 - $2*10^5$	10^3 - 10^5	10^3 - 10^5	10^3- 10^5

Table VI: Properties of MASCOT reference soils. See [19] for a detailed explanation of the parameters listed here.

IV.IV. MBS simulation results

Dynamic analysis was performed using MBS simulation. Different scenarios and parameter variations lead to design proposals and first component suggestions. Results of the excenter tappet concept analysis are presented in the following.

Model parameters

The MASCOT MBS model, as shown in Fig. XIX, consists of five bodies: The MASCOT structure, the actuator (motor-gear unit), the two actuator masses and a payload dummy.
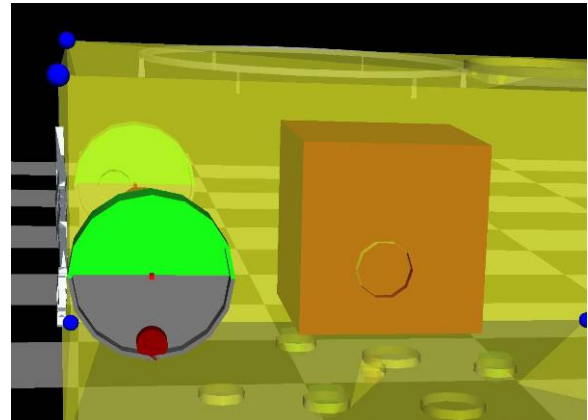

Fig. XIX: Model components: In the foreground one excenter mass (actuator unit hidden); the payload dummy inside the semi-transparent structure.

The structure represents the cover and defines MASCOT's contact body. The parallel rotation of the excenter masses is realized by giving a defined rotation on the actuator unit, which is rigidly connected to both of them. As payload dummy a mass is placed in MASCOT's CoM (Centre of Mass) and connected to the model with a certain flexibility, to

represent the inner elasticity of the payload. The overall mass of the model is 10 kg; the inertial tensor is estimated from mass, shape and assumed mass distribution.

The asteroid is modelled as a homogeneous sphere, shown in Fig. XX, with a diameter of 920 m, optional 980 m. A density of 1300 kg/m³ [10] is assumed. Frome there, the gravitational force can be easily computed, according to the explanations in section III.II, by calculating the asteroid's mass and the distance from MASCOT's CoM to the asteroids center in every integration step.

The small sphere over the north pole of the asteroid in Fig. XX is a massless virtual sphere (diameter: 20 m), attached to the MASCOT structure. Because of MASCOT's very small size, it helps to visualize its position and attitude in overall view.

Fig. XX: Asteroid model

Contact models

Two contact models are used for contact force analysis: The Polygonal Contact Model (PCM) for rigid contact and the Soil Contact Model (SCM) for contact on soft, sandy terrain. Both contact models can work parallel in one model, if needed.

The most important parameters of PCM are listed in Table VII. The given standard values can vary for different scenarios.

Parameter	Value	Source
Young's modulus / [N/m^2]	4.72e5	Tests (IV.III)
Poisson ratio	0.4	[19]
Layer depth / [m]	0.02	[19]
Areal damping / [Ns/m^3]	1.0e7 - 1.0e9	Simulation, research
Damping depth / [m]	0.02	[19]
Friction coefficient μ	0.45	[19], research

Table VII: PCM parameters

For PCM, the contact bodies are defined as polygons and the forces are computed by analyzing the virtual intersection of the bodies [20]. Multiple contacts between almost arbitrarily shaped bodies are possible. For MASCOT, PCM is suitable for most analyses of dynamic behaviour.

Additional parameters, which describe the soil behaviour, are needed for SCM. The values are identified by tests and are conform to the parameters of section IV.III; they are given in Table VI.

The SCM contact model offers the possibility to apply the terramechanics theory of Bekker [19] and Wong [21] with MBS simulations. It has been developed by DLR-RM for planetary rover dynamic wheel-soil interaction calculation [22]. For MASCOT, it is used to analyze special scenarios on soft soil and sandy terrain.

Functional analysis

The functionality of the system is based on the angular impulse-momentum principle. An excentric mass rotates on a tappet around a pivot. The motor, connected to the axis, is able to accelerate the mass in a defined way and on the other hand to bring it to a defined stop. The control of start and stop angle and the values of acceleration and deceleration are supported by micro-positioning sensors.
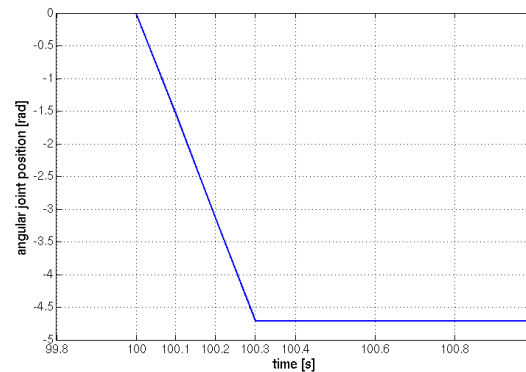

Fig. XXI: Typical actuator input (detailed time span)

Fig. XXI shows an extract of the motion phase of a typical actuator sequence as angle (rad) over time. The mass is accelerated from $t = 100.0$ s to $t = 100.3$ s. During the acceleration phase the axle turns clockwise from initial position to -4.7 rad or -270 deg. In this phase, following the actio-reactio principle, the MASCOT structure is accelerated counterclockwise and therefore slightly pressed into the ground. This acceleration is absorbed in the structure-soil contact and does not cause any turnaround motion. After that, at 100.3 s, it comes to an abrupt stop of axle and mass. Due to the inertia of the rotating mass, a peak momentum is transmitted to the MASCOT structure. Therefore the structure is brought to rotation by a impulse dependent on the defined stop angle of the actuator. The acting impulse change ΔP is the product of the excenter mass m_{exc} and the tangential velocity change Δv:

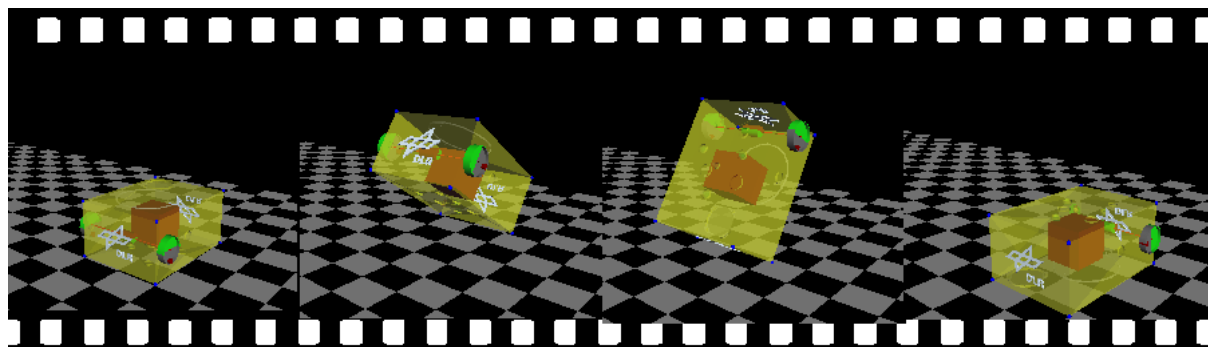$$\Delta P = m_{exc} \cdot \Delta v_{\tan} \qquad [4]$$

Fig. XXII: Upright sequence; turnaround (from left to right)

The tangential velocity change Δv directly depends on the angular speed change $\Delta \omega$, which results from the applied power of the actuator unit. By varying the application power in combination with different start- and stop-angles, the direction as well as the applied energy can be adjusted to set up the resulting movement.

To analyze the functionality of the proposed mobility system, a multitude of scenarios with different configurations and varied input parameter sets are simulated. The result parameters of these simulations extend from contact forces, torques, and attitude parameters (position, rotation angle) of all bodies to visualizations as well as data for further investigation, e.g. power consumption calculation.

Fig. XXII shows a typical movement sequence as visualized result of one simulated upright scenario. Visualizations in general provide a fast understanding of the dynamic model behaviour.
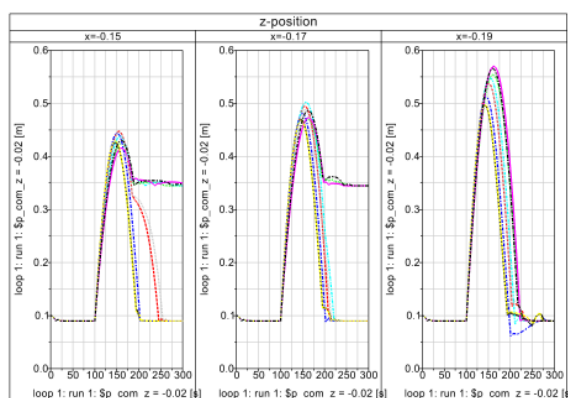

Fig. XXIII: Parameter variation: z-position

One advantage of simulation is the possibility of a fast sensitivity analysis of a system to changing conditions. For MASCOT, a parameter variation of the system behaviour with displaced CoMs was performed.

Fig. XXIII shows the z-positions of the MASCOT structure as indicator of a successful turn-around. If the reference point comes to similar start- and end-positions, a turn-around about 180 deg can be assumed. The result can be assured e.g. by regarding the rotation angles. Each of the three diagrams in Fig. XXIII shows a displacement of +/-0.02 m of the CoM

in y- and z-direction and three fixed x-positions. It is obvious that the x-position of x = -0.19 m from the front plate shows less sensitivity to the x- and y-displacement than the other x-positions, where some combinations obviously do not lead to a successful turnaround. All numerical integrations are performed with the same input sequence, compared to Fig. XXI.

Design support/component selection

The simulation results are used to provide design support and give suggestions for suitable components of the mobility system.
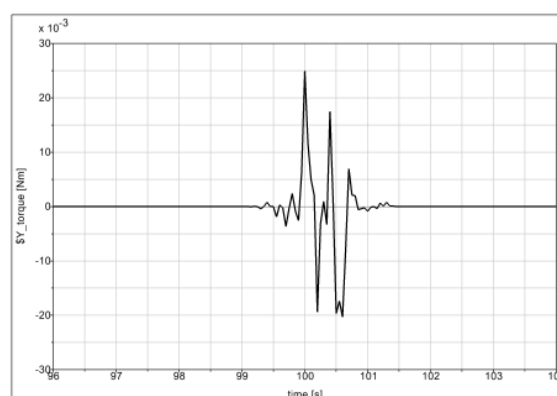

Fig. XXIV: Actuator torque (detailed time span)

In Fig. XXIV the progression of the needed actuator torque for one uprighting action is shown. This kind of diagram is used to define the suitable motor-gear combination with respect to maximum torque and responding behaviour (see also section IV.V.).

Example scenario

Two additional results of a hopping scenario on the asteroid (diameter 980 m) are presented. The scenario has a numerical run time of 1500 s, in which the actual hop happens between t = 300 s and t = 760 s.

The z-position, which means the altitude over the asteroid's surface, as well as the gravitational force acting on MASCOT, are both presented in Fig. XXV. It shows clearly the dependence of the gravitational force from the distance of MASCOT to the asteroid's center. As the acting gravitational force is calculated by the software for each integration step, this indicates the correct work of the gravitation model.
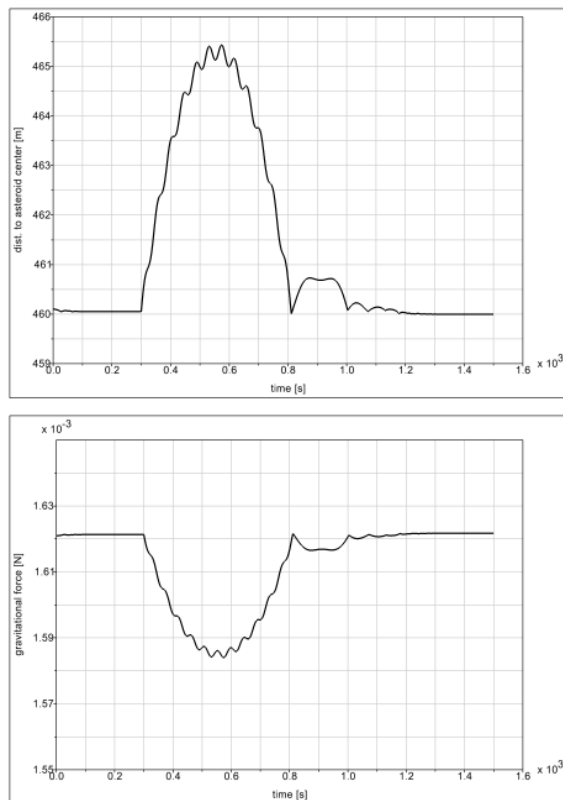
Fig. XXV: Altitude, z-position (above) and gravitational force (below) during hopping

The exemplary hop has an absolute altitude of about 5.0 m, which results in an absolute position change over ground of approximately 3.5 m. In Fig. XXVI the absolute position on the asteroid surface layer is presented, calculated from the x- and y-position wrt. the asteroid's coordinate system. MASCOT's start position has an offset of 1.0 m from this coordinate system; the waved line indicates a rotation of the structure during the flight.
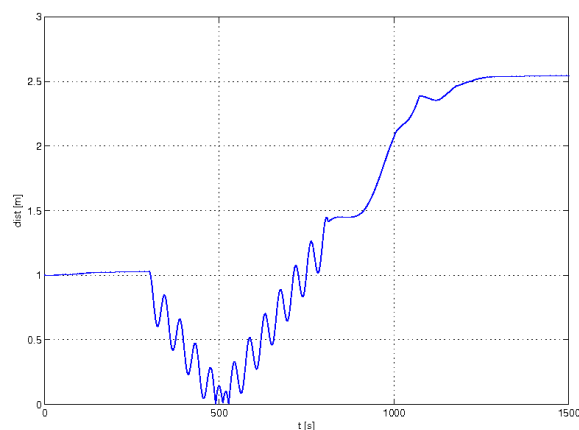

Fig. XXVI: Absolute position over ground of MASCOT during hopping

IV.V. Components

The described results of the performed simulations are applied to the design development and the preselecting of components.

Motor unit

A suitable motor for MASCOT based on its power and control specifications as well as its sensor system is the ILM25. Originally, the light-weight and high performance brushless DC motor type has been developed at DLR Oberpfaffenhofen, but is now commercially available by the company RoboDrive [23]. It is a three-phase brushless DC motor with three Hall sensors for commutation. The appropriate gear is a Harmonic Drive HFUC 8. A ratio of 30:1 with an output torque of up to 1.0 Nm is adequate for the needs of MASCOT, according to Fig. XXIV.

In Fig. XXVII, the CAD assembly of the actuator unit inside the MASCOT structure is shown.
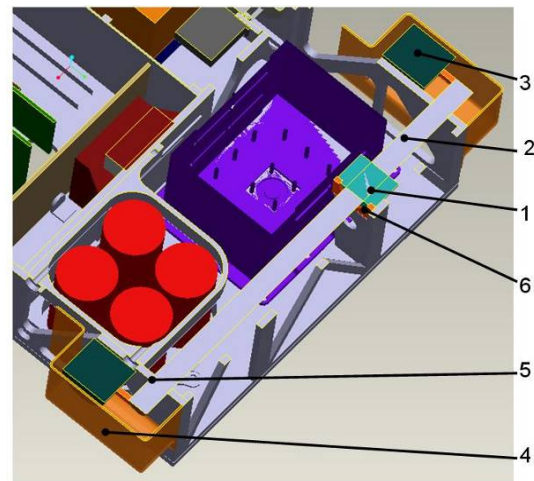

Fig. XXVII: Mobility System Components

Basically the mechanism consists of the motor-gear unit (1) and an axle (2), which transmits the torque to the inertia masses (3) on both sides of MASCOT. These masses are located outside the inner structure of MASCOT for package reasons, although they are protected by a cover (4). The transmission axle is mounted in sealed ball bearings (5). A mounting plate (6) supports the motor-gear unit to the MASCOT structure.

Electronics and Controller

Allegro A3930 motor controller is the central component of the electronic subsystem. This is a fully integrated and very flexible three-phase motor controller, which integrates MOSFET drivers and a number of application and safety features. The design of the controller system is based on DLR Oberpfaffenhofen's long-term experience with the ROKVISS actuator arm experiment on the outer surface of the ISS [24]. The power electronic is estimated to be mounted inside MASCOT's shielded electronic box. Therefore it is on a standard interface board with a local power supply.

V. OUTLOOK

The MASCOT phase-A study work was successfully completed in the end of July 2010. Currently, phase B begins, which mainly comprises

breadboarding and test activities. While the landing simulations already yielded to comprehensive results, extensive testing of the mobility mechanism due to the challenging environment like very low gravity and mostly unknown surface properties is necessary.

Therefore, a mock-up is planned for testing and demonstrating the functionality of the mobility system. This mock-up has to be much scaled in dimensions as well as in component properties to provide testable motion behavior under earth gravitation. A following functionality breadboard is intended to be built, with the dimensions and electronic components of the flight model. A sensor-based testing strategy is then needed because of its concept made for 10^{-5}g.

All breadboarding activities and future analysis are supported by more detailed and further developed MBS simulations. With the results of these, a potential optimization of the mobility system concerning the mass and excenter dimensions as well as the dynamic behavior seems possible. The final selection of components is also a process, which can benefit from these results.

Project planning foresees a phase-B study till end of March 2011 to be compatible to the HAYABUSA-2 flight opportunity in 2014. The subsequent study work will focus on a more detailed and optimized subsystem design, while in parallel the final payload selection process will be initiated with close collaboration of all national and international partners.

VII. REFERENCES

[1] Ulamec, S., Biele, J.: Surface elements and landing strategies for small bodies missions – Philae and beyond, Advances in Space Research 44, page 847-858, 2007

[2] Yoshimitsu, T. et al.: Micro-hopping robot for asteroid exploration, Acta Astronatuica 52, page 441-446, 2003

[3] JAXA Space Exploration Center Homepage, request July 2010, http://www.jspec.jaxa.jp/e/activity/hayabusa2.html

[4] Ho T.-M. et al.: MASCOT Science Requirement Document, Iss. 1, Rev. 1, DLR Report, 2009

[5] Lange, C. et al.: Baseline Design of a Mobile Asteroid Surface Scout (MASCOT) for the Hayabusa-2 Mission, 7th International Planetary Probe Workshop Proceedings, Barcelona, Spain, 14-18 June 2010

[6] Kawaguchi, J. et al.: Orbit Synthesis for Hayabusa-2 and Marco Polo (Hayabusa MK-II) primitive bodies sample return missions, IAC-080C1.2.9, 2008

[7] Abe, S. et al.: Physical property of 162173 1999JU3 estimated by ground-based observations; International Symposium Marco Polo and other Small Body Sample Return Missions, May 18-20, 2009

[8] MASCOT-DK CE-study, CEF DLR Bremen, January 2010

[9] MASCOT Thermal Analysis Document, MASCOT-XS Thermal Analysis, Active Space Technologies GmbH, AST-MASCOT-RP-5203, February 2010

[10] Bellerose, J. et al.: Dynamics of Asteroid 1999 JU3 : Target of the Hayabusa Follow-on Mission, 2009-k-03

[11] Abe, M. et al.: Ground-based observational campaign for asteroid 162173 1999 JU3, Lunar and Planetary Science XXXIX, 2008, 1594.pdf

[12] Hasegawa, S. et al.: Albedo, Size, and Surface Characteristics of Hayabusa-2 Sample-Return Target 162173 1999 JU3 from AKARI and Subaru Observations, PASJ 60, S. 399-405, 2008

[13] Numerical Recipes: The Art of Scientific Computing, Third Edition, Cambridge University Press, 2007

[14] Bellerose, J., Scheeres, D.J.: Stability of equilibrium points in the restricted full three-body problem, Acta Astronautica 60, page 141-152, 2007

[15] Bellerose, J. et al.: Progress Report – Landing Analysis for the Marco Polo mission, March 2009

[16] Yano, H. et al.: Touchdown of the Hayabusa Spacecraft at the Muses Sea on Itokawa, Science Vol. 312, page 1350-1353, 2006

[17] JPL Small-Body Database, request July 2010, http://ssd.jpl.nasa.gov/sbdb.cgi

[18] Richter, L. et al.: Marco Polo Surface Scout (MASCOT) – Study of an Asteroid Lander for the Marco Polo Mission, IAC-09-A3.5.5, IAC, 2009

[19] Bekker, M.G.: Theory of Land Locomotion, University of Michigan Press, second edition, 1956

[20] Hippmann, G., Modellierung von Kontakten komplex geformter Koerper in der Mehrkoerperdynamik, Dissertation, TU Wien, 2004.

[21] Wong, J.Y.: Theory of Ground Vehicles, J. Wiley, third edition, 2007

[22] Schaefer, B., Gibbesch, A., Krenn, R., Rebele, B., Planetary rover mobility simulation on soft and uneven terrain, Vehicle System Dynamics, 48:1, 149-169, 2010

[23] Robodrive website, request July 2010, http://www.robodrive.de

[24] Preusche, C.; Reintsema, D.; Landzettel, K.; Hirzinger, G.: Robotics Component Verification on ISS; ROKVISS - Preliminary Results for Telepresence. IEEE Proceedings, p. 4595-4601. IROS 2006, Beijing, China, 2006